Clay Minerals, (2018) **53**, 143–158

Application of chlorite thermometry to estimation of formation temperature and redox conditions

ATSUYUKI INOUE[1,*], SAYAKO INOUÉ[2] AND MINORU UTADA[3,†]

[1] *Chiba University, Chiba 263-8522, Japan*
[2] *Department of Geosciences, Virginia Tech, Blacksburg, VA 24061, USA*
[3] *Futo, Ito, Shizuoka 413-0231, Japan*

(*Received 5 October 2017; revised 3 March 2018; Guest Associate editor: V. Trincal*)

ABSTRACT: Diverse applications of chlorite thermometry have been considered for better understanding the formation process in nature. Here, an approach which combined a semi-empirical thermometer (Inoue *et al.,* 2009) with the method of Walshe (1986) was tested to estimate the redox conditions (log f_{O_2}) and the formation temperature, using the literature data from Niger, Rouez and St Martin and new data for chlorite which coexists with pink-coloured epidote in the Noboribetsu geothermal field. The log f_{O_2} predicted for the former data sets were compatible with those estimated by Vidal *et al.* (2016), suggesting that the present approach is valid for quantifying the variations in log f_{O_2}. The Noboribetsu chlorites have lower Fe/(Fe + Mn + Mg) and greater $Fe^{3+}/\Sigma Fe$ ratios than those observed in adjacent propylite rocks. The peculiar mineral assemblage and chemical composition are attributed to the formation under higher f_{O_2} conditions and possibly low Fe concentration in the alteration fluids.

KEYWORDS: chlorite thermometry, redox conditions, hydrothermal alteration, pinkish epidote.

Chlorite is a common mineral which occurs in a wide range of geological environments such as diagenesis, low- to medium-grade metamorphism and hydrothermal alteration. The mineral exhibits a wide range of compositional variations in response to the changes in ambient physicochemical conditions during formation, which include temperature (T), pressure (P) and redox conditions in addition to the bulk-rock and fluid compositions. Hence, it is expected that these physicochemical conditions may be estimated from the chemical compositions of end-product chlorite and coexisting minerals as has been shown in previous studies.

Three types of the single-mineral thermometry have been developed to estimate the formation temperature of chlorite: the so-called empirical Al(IV)-in-chlorite (*e.g.* Cathelineau & Nieva, 1985; Cathelineau, 1988; Kranidiotis & McLean, 1987; Jowett, 1991; Hillier & Velde, 1991; Zang & Fyfe, 1995), rigorous thermodynamic thermometers (Vidal *et al*., 2001, 2006; Lanari *et al.,* 2014) and semi-empirical thermometers (Walshe, 1986; Inoue *et al.,* 2009; Bourdelle *et al.,* 2013; Lanari *et al.,* 2014). Detailed comparison of the three types of thermometers has been presented in previous reviews (*e.g.* De Caritat *et al.,* 1993; Essene, 2009; Inoue *et al.,* 2009, 2010; Bourdelle & Cathelineau, 2015; Vidal *et al.,* 2016) and will not be repeated here. Nevertheless, there are some points to be considered. First, electron microprobe analysis (EPMA) cannot separate ferric from ferrous Fe in chlorite. Therefore, for simplicity of

This paper was presented during the session: 'MI-04: Diversity of chlorites' of the 2017 International Clay Conference
*Email: atinoue@earth.s.chiba-u.ac.jp
https://doi.org/10.1180/clm.2018.10
†Deceased

Copyright © Mineralogical Society of Great Britain and Ireland 2018
https://doi.org/10.1180/clm.2018.10 Published online by Cambridge University Press

data processing, the semi-empirical thermometers proposed by Bourdelle *et al.* (2013) and Lanari *et al.* (2014) assumed $\Sigma Fe = Fe^{2+}$, suggesting that the data determined by EPMA are directly usable in these thermometers. On the contrary, the other semi-empirical thermometers (Walshe, 1986; Inoue *et al.,* 2009) and rigorous thermodynamic thermometers (Vidal *et al.,* 2005, 2006; Lanari *et al.,* 2014) required the $Fe^{3+}/\Sigma Fe$ ratios to estimate the formation temperature. The latter approaches have an advantage that the determination of $Fe^{3+}/\Sigma Fe$ ratios enable us to estimate the oxygen gas fugacity (f_{O_2}) conditions in addition to the formation temperature (Walshe & Solomon, 1981; Walshe, 1986; Vidal *et al.,* 2016). Secondly, the thermodynamic and the semi-empirical methods, but not the empirical methods, gave apparently comparable estimates for the formation temperature of low-temperature chlorites, although the estimates did not always match perfectly. This is because the data source used and the activity models assumed were different in calibrating respective thermometers.

The present study aimed to estimate f_{O_2} conditions during chlorite formation, together with the formation temperature, by combining the semi-empirical thermometer of Inoue *et al.* (2009) with the method proposed by Walshe (1986). The study consists of two sections: in the first, the validity of the present approach is demonstrated through comparison with the results of Vidal *et al.* (2016), using data from chlorites from Niger, Rouez and St Martin (Inoue *et al.,* 2009). In the second section the same approach was applied to recently published data on chlorites coexisting with pink-coloured epidotes in the Noboribetsu geothermal field (Inoue & Utada, 2017). Previous studies of regional metamorphism (*e.g.* Keskinen & Liou, 1979; Kawachi *et al.,* 1983; Bonazzi & Menchetti, 2004) have shown that reddish piemontite (manganian epidote) formed under oxidizing conditions. However, the formation conditions of pinkish to reddish epidote in hydrothermal environments are poorly understood because of the scarcity of occurrence compared to piemontite in regional metamorphism (Deer *et al.,* 1986). Our final goal here was to characterize the variations in chemical composition of chlorite which formed with pinkish epidote under oxidized conditions and to clarify the role of f_{O_2} during chlorite formation along with the formation process based on other physicochemical conditions.

CHLORITES FROM NIGER, ROUEZ AND ST MARTIN

Firstly, the two methods proposed by Walshe (1986) and Vidal *et al.* (2016) were tested to estimate oxygen gas fugacity (f_{O_2}) conditions using the literature data for chlorites from the Niger, Rouez and St Martin areas. Chlorites in Niger and St Martin occur in diagenetic sandstones and hydrothermally altered rocks, respectively, whereas their Rouez counterparts occur in low-grade metamorphic rocks surrounding a massive sulfide deposit. A detailed mineralogical description of the chlorites can be found in Inoue *et al.* (2009) and references therein. The sets of data are worthy because the $Fe^{3+}/\Sigma Fe$ ratios in chlorites have been determined by Mössbauer spectroscopy, the formation temperatures have been estimated (Inoue *et al.,* 2009) and the results have been evaluated extensively by later works (*e.g.* Bourdelle *et al.,* 2013; Lanari *et al.,* 2014; Bourdelle & Cathelineau, 2015; Vidal *et al.,* 2016).

Estimation of f_{O_2} conditions

Walshe (1986) introduced an endmember component of H-deficient Fe^{3+}-chlorite $Fe_4^{2+}Fe^{3+}Al_2Si_3O_{11}(OH)_7$ in chlorite solid solution. The presence of the H-deficient Fe^{3+}-chlorite component cannot be ascertained by the usual microprobe analysis (Vidal *et al.*, 2016), but the universal presence of less than stoichiometric H^+ in chlorites has been ascertained by Mössbauer spectroscopy (*e.g.* Dyar *et al.,* 1992, 1993).

The oxidation-dehydration reaction of chamosite $Fe_5^{2+}Al_2Si_3O_{10}(OH)_8$ to H-deficient Fe^{3+}-chlorite $Fe_4^{2+}Fe^{3+}Al_2Si_3O_{11}(OH)_7$ is described by:

$$Fe_5^{2+}Al_2Si_3O_{10}(OH)_8 + 1/4O_2(g) = Fe_4^{2+}Fe^{3+}Al_2Si_3O_{11}(OH)_7 + 1/2H_2O(l) \quad (1)$$

The relationship between temperature and the equilibrium constant $K_{(1)}$ of reaction 1 was given by Walshe (1986):

$$\log K_{(1)} = -1.926 + 6075.8/T \quad (2)$$

where T is temperature in degrees Kelvin. Assuming that the activity of water, $a_{H_2O} = 1$, the logarithmic oxygen gas fugacity ($\log f_{O_2}$) for reaction 1 is described as follows:

$$\log f_{O_2} = 4\left[\log a_6 - \log a_3 - \log K_{(1)}\right] \quad (3)$$

where a_3 and a_6 are the activities of chamosite and H-deficient Fe^{3+}-bearing chlorite components in reaction 1, respectively. The ideal activity terms of the two components can be calculated with the mixing-on-sites model (*e.g.* Powell, 1978) when the $Fe^{3+}/\Sigma Fe$ ratios are known, ignoring the non-ideality effects of solid solution. The model of ideal activity for chamosite

https://doi.org/10.1180/clm.2018.10 Published online by Cambridge University Press

component (a_3) is identical to that of Walshe (1986) and Inoue *et al.* (2009): $a_{\text{chamosite}} = 59.720(X_{Fe^{2+},oct})^5 (X_{Al,oct})(X_{Si,tet})(X_{Al,tet})$, where X_i is a site fraction of the *i* ion occupying the octahedral (oct) or tetrahedral (tet) sites. The ideal activity of the H-deficient Fe^{3+}-bearing chlorite component (a_6) was calculated from: $a_6 = X_6$, where X_6 is a mole fraction of $Fe_4^{2+}Fe^{3+}Al_2Si_3O_{11}(OH)_7$ component in chlorite. In this work, different assumptions from Walshe (1986) were adopted to calculate X_6. The practical procedures of calculation are given in the Appendix at the end of this paper. Log f_{O_2} values were calculated from equation 3 using the data for formation temperatures already estimated by the thermometer proposed by Inoue *et al.* (2009), log $K_{(1)}$ was calculated from equation 2 and the chemical compositions containing data for the $Fe^{3+}/\Sigma Fe$ ratio. The calculated log f_{O_2} values are plotted as a function of the formation temperature at the vapour-liquid equilibrium pressure for water ($P_{\text{sat L/V}}$) (Fig. 1a).

Vidal *et al.* (2016) also estimated the activities of oxygen (a_{O_2}) in fluids during the formation of chlorites in Niger, Rouez and St Martin, assuming that they were buffered by pure magnetite in equilibrium with chlorite + quartz at $P = 2$ kbar (Fig. 1b). Their calculations were rigorous taking into consideration the non-ideal activity effects of solid solution. Some chlorites were discarded from the calculations because the method is restricted to chlorites with Si < 3 atoms per half formula unit (a.p.h.f.u., Vidal *et al.*, 2001). In fact, a number of chlorites with Si > 3 were contained in the data set. Nevertheless, it is obvious that the two plots in Fig. 1 are similar to one another.

The fact that apparently hematite-free samples were plotted in the hematite stability field of log f_{O_2} implied that the calculated log f_{O_2} values were too high or that oxygen was not buffered by an equilibrium of magnetite with chlorite (Vidal *et al.* 2016). A new endmember ferri-sudoite was introduced in the chlorite solid solution and the f_{O_2} conditions were recalculated for reactions without magnetite. The introduction of a ferri-sudoite endmember led to a reasonable result for the Rouez samples (Vidal *et al.*, 2016). Similarly, in reaction 1, where the presence of any oxide minerals was not considered, it was predicted that the samples from Rouez and Niger should plot in the magnetite stability field of log f_{O_2} and on the hematite–magnetite equilibrium curve, respectively (Fig. 1a). The results are consistent with the mineral assemblages documented from the two fields (Inoue *et al.*, 2009). The log f_{O_2} for the St Martin samples are also arrayed so as to be compatible with the reported mineral assemblages (Beaufort *et al.*, 1992).

Effect of pressure

Different pressure values were assumed in the aforementioned calculations. The effect of different

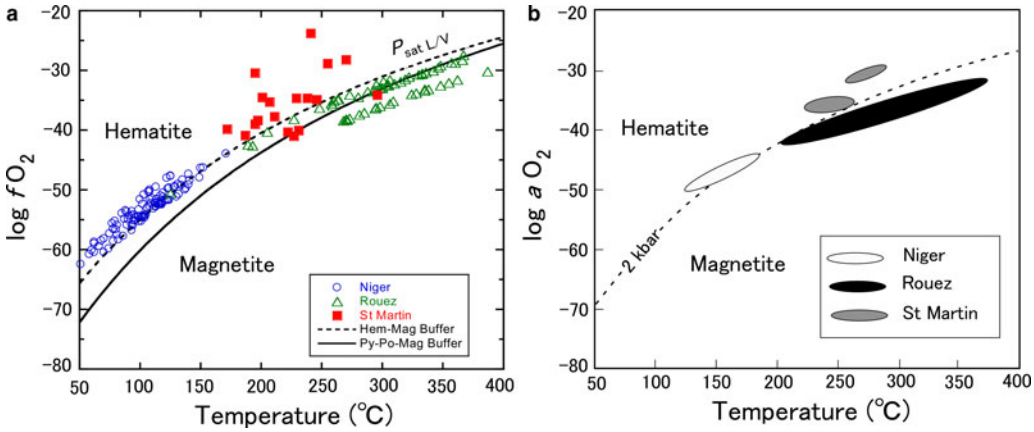

FIG. 1. Comparison of log f_{O_2} *vs.* temperature for Niger, Rouez and St Martin samples. (a) log f_{O_2} and formation temperatures were calculated at $P_{\text{sat L/V}}$ using the approaches of Walshe (1986) and Inoue *et al.* (2009), respectively. Dashed and solid curves are the hematite–magnetite equilibrium and the pyrite–pyrrhotite–magnetite equilibrium curves calculated at $P = P_{\text{sat L/V}}$ using the thermodynamic data of Lonker *et al.* (1990) and Walshe & Solomon (1981), respectively. (b) Reproduced from Fig. 8 of Vidal *et al.* (2016) after partial modification with the permission of the Mineralogical Society of Great Britain & Ireland.

https://doi.org/10.1180/clm.2018.10 Published online by Cambridge University Press

pressures can be evaluated from the following relationship (*e.g.* Bryndzia & Scott, 1987):

$$\log Kp_2 - \log Kp_1 = -\Delta V_s^o (P_2 - P_1)/2.303RT \quad (4)$$

where ΔV_s^o denotes the difference in molar volumes of solid phases at the standard state, Kp_1 and Kp_2 are the equilibrium constants at pressures P_1 and P_2, and R and T are the gas constant and temperature in degrees Kelvin, respectively. Following the molar volume data given by Walshe (1986), the ΔV_s^o between chamosite (ΔV^o = 213.42 cm^3/mole) and H-deficient Fe^{3+}-chlorite (ΔV^o = 214.4 cm^3/mole) was very small (ΔV_s^o = 0.098 J/bar/mole) suggesting that the pressure effect was insensitive in the model of Walshe (1986). On the other hand, the molar-volume changes (ΔV_s^o) in reactions 11–23 of Vidal *et al.* (2016) ranged from –7.6 to 57.4 J/bar/mole, which varied with the adopted reaction. Taking into account the stoichiometric coefficients of oxygen gas in the Vidal *et al.* (2016) reactions 11–23, however, final changes in $\log f_{O_2}$ with respect to different pressures were also insensitive to the reactions. As a consequence, the entire array of two plots shown in Fig. 1 is not affected significantly by assuming different pressures. Rather, the differences in formation temperature estimated by both Inoue *et al.* (2009) and Vidal *et al.* (2016) influence the estimated $\log f_{O_2}$. In general, the lower the temperature, the lower the calculated $\log f_{O_2}$ value.

Redox buffers in closed systems

Oxygen acts as an immobile (inert) component in regional metamorphism (Thompson, 1957; Chinner, 1960; Banno & Kanehira, 1961; Miyashiro, 1965). Therefore, if f_{O_2} is controlled internally by the assemblage chlorite + magnetite, then the Fe/(Fe + Mg) ratio of chlorite should be inversely correlated with modal magnetite, because the Fe to form magnetite is supplied by chlorite (Frost, 1991), as exemplified by reaction 5 below:

$$\begin{aligned} &6\text{Chamosite} + 4\text{Clinochlore} + 5O_2 = 5\text{Mg-Corundophilite (or Amesite)} + 10\text{Magnetite} + 20\text{Quartz} \\ &20H_2O6Fe_5Al(Si_3Al)O_{10}(OH)_8 + 4Mg_5Al(Si_3Al)O_{10}(OH)_8 + 5O_2 = 5Mg_4Al_2(Si_2Al_2)O_{10}(OH)_8 + 10Fe_3O_4 + 20SiO_2 + 20H_2O \end{aligned} \quad (5)$$

This reaction has been documented in metamorphic rocks (*e.g.* Chinner, 1960; Frost, 1991) and metamorphosed ore deposits (*e.g.* Banno & Kanehira, 1961; Kanehira *et al.,* 1964; Nesbitt, 1986; Bryndzia & Scott, 1987). In reality, the situation is more complex in chlorite that receives Fe^{3+} because of the coupled substitutions necessary to maintain charge balance (Frost, 1991). The information about the modal contents of oxide minerals is not reported in the three fields studied here. Meanwhile, the occurrence of authigenic magnetite is generally scarce in diagenesis and hydrothermal alteration under low-T conditions. Rather, hematite and/or pyrite instead of magnetite occur more commonly in such environments. Pyrite and pyrrhotite possibly act as redox-controlling minerals with oxides at relatively higher temperatures in a closed system (*e.g.* Banno & Kanehira, 1961; Kanehira *et al.,* 1964; Nesbitt, 1986; Bryndzia & Scott, 1987). The chlorite + sulfide assemblage associated with oxide minerals might act as a main buffer assemblage which controlled the redox conditions in Rouez because of the abundant occurrence of sulfides (Beaufort, 1986). Indeed, the pyrite–pyrrhotite–magnetite buffer reduces log f_{O_2} from the hematite–magnetite buffer and appears to control the redox conditions in Rouez (Fig. 1a). However, in St Martin, the chlorites coexisting with magnetite in veins were richer in Fe than those without magnetite or with hematite (Beaufort *et al.,* 1992). This behaviour is not expected by the hypothesis above and may be due to the fact that the f_{O_2} was controlled externally in the St Martin hydrothermal system, similar to the Noboribetsu system (see next section). If hematite was stable instead of magnetite, Fe-chlorite would alter to Mg-chlorite and finally to sudoite depending on the Mg-availability in the system, because trioctahedral chlorite cannot host large amounts of Fe^{3+} in the structure. Chlorites in Niger are relatively rich in Fe (Fe/(Fe + Mg) ratio = 0.59 on average), and it is possible that oxygen was not buffered by an equilibrium of oxides with chlorite. Despite the somewhat ambiguous prediction of log f_{O_2}, it is conclusive that the present approach might be utilized to estimate the redox conditions during chlorite formation.

CHLORITES FROM NOBORIBETSU

Petrographic descriptions of the samples studied

The geological setting, hydrothermal alteration and thin sections of the cores studied were described by Inoue & Utada (2017). Briefly, the core samples

https://doi.org/10.1180/clm.2018.10 Published online by Cambridge University Press

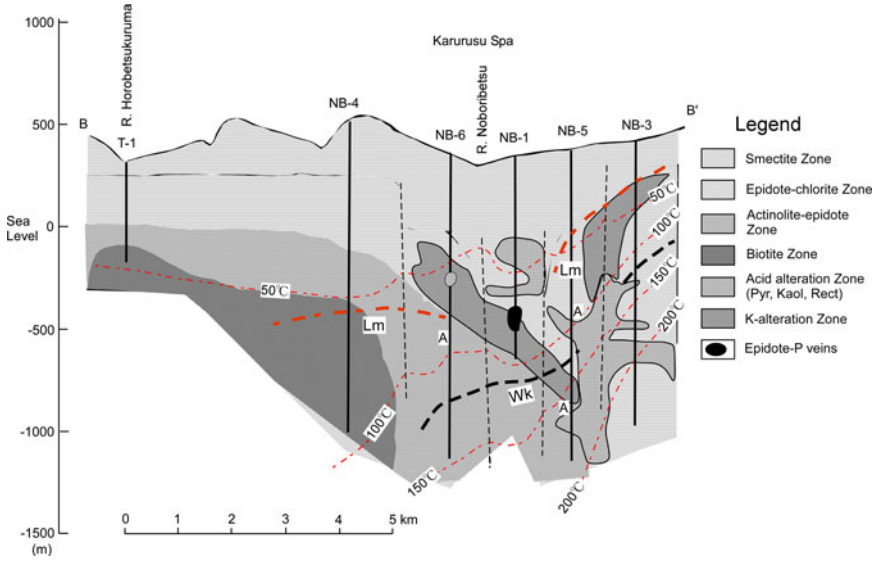

FIG. 2. A cross-section showing the distribution of hydrothermal alteration zones. The cores studied were collected from the part of NB-1 marked with black. Thin dashed lines denote the distribution of present subsurface temperature. Thick dashed lines denote the appearance depths of laumontite (Lm) and wairakite (Wk), respectively. A: depths at which analcime was identified (adapted from Inoue & Utada, 2017 and reproduced here with the permission of The Japanese Mineralogical Society).

studied were collected from a geothermal exploration hole NB-1 in the Noboribetsu area (Fig. 2). Hydrothermal alteration in this area is divided into several types of alteration that took place at different stages. The underlying pre-Tertiary and Miocene rocks underwent early propylitic alteration that consists of biotite, actinolite-epidote and epidote-chlorite zones (Fig. 2). The overlying Quaternary volcanic rocks were altered to smectite and halloysite, whereas some unaltered glass remained in the rocks. Early propylitic alteration was overprinted locally by later Ca zeolitization, potassic alteration and advanced argillic alteration characterized by the presence of pyrophyllite, kaolinite and rectorite. The potassic alteration was diagnostic of the presence of abundant K-feldspar and illite, in addition to pinkish epidotes and brownish chlorites of interest in the present study.

Seven core samples of Hole NB-1, two pinkish epidote-bearing rocks at depths of 837.4 and 897.7 m and five adjacent rocks with propylitic alteration at depths of 792.7, 808.9, 880.5, 888.2 and 996.5 m, were examined in the present study. Pink-coloured epidotes (abbreviated hereafter as epidote-P) occurred as vein fillings and druses in rocks (Fig. 3a). Fine-grained epidote-P was also pervasive in the matrix of wholly silicified rock in the sample at 897.7 m in which original albite was completely decomposed by the overprinted potassic alteration. At 837.4 m, epidote-P occupied veins associated with adularia-like K-feldspar and quartz (Fig. 3b). Green-coloured chlorite (denoted hereafter as chlorite-G) was crosscut by a veinlet of brown-coloured chlorite (denoted hereafter as chlorite-B) (Inoue & Utada, 2017). Titanite and hematite were common in the samples at 837.4 m and 897.7 m. White to mottled brown-coloured apatite was identified in the samples at 792.7, 808.9 and 888.2 m, which is the product of potassic alteration. In contrast, epidotes with a greenish colour (denoted hereafter as epidote-G) replaced plagioclase and filled veins and druses in rocks with propylitic alteration and usually coexisted with chlorite-G, *e.g.* in the sample at 792.7 m. However, in these rocks, chlorites were surrounded by dark brown rims and/or partially replaced by brown illite (Fig. 3c), as was shown by microprobe analysis (Inoue & Utada, 2017). Chlorite-B in the sample at 837.4 m included titanite and pyrite grains (Fig. 3d). The pyrite grains were rimmed by fine-grained epidote. Actinolite was identified in the sample at 996.5 m. Although small amounts of carbonates were observed in the studied rocks, the stage of carbonate-mineral formation remains uncertain.

https://doi.org/10.1180/clm.2018.10 Published online by Cambridge University Press

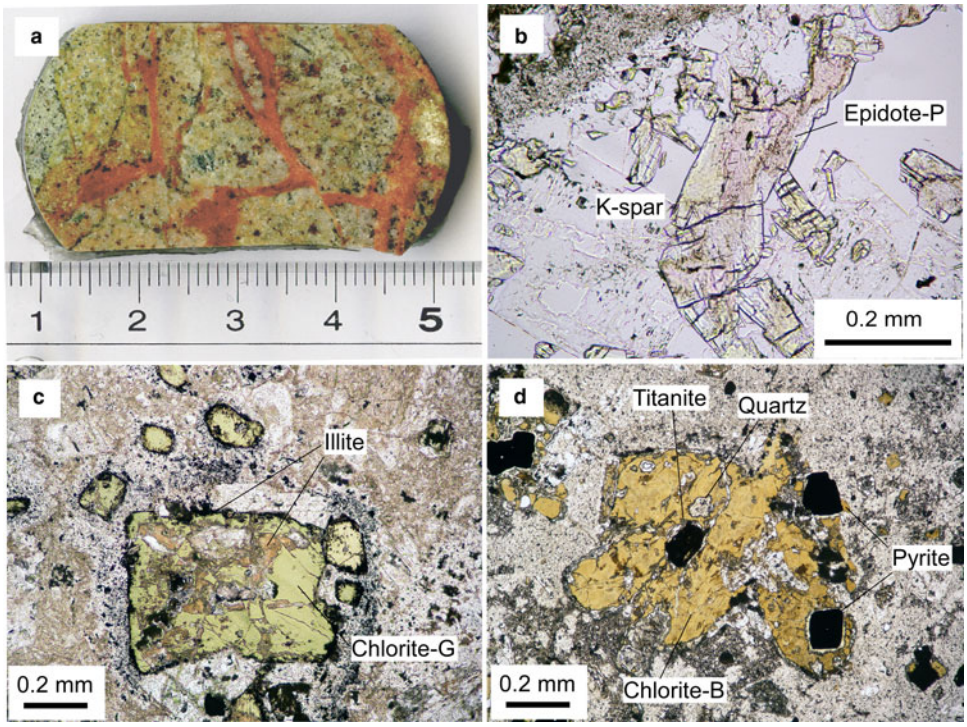

FIG. 3. (a) Core sample with pinkish epidote veins from 897.7 m; (b) a pinkish epidote grain (epidote-P) showing a sector zoning under plane polarized light (837.4 m), K-spar: K-feldspar; (c) greenish chlorite (chlorite-G) rimmed by dark brown illite and partially replaced by brownish illite, under plane polarized light (808.9 m); (d) brownish chlorite (chlorite-B) associated with titanite in the centre and pyrite with colourless epidote rims to the right of chlorite (837.4 m) (modified from Inoue & Utada, 2017 and reproduced here with the permission of The Japanese Mineralogical Society).

Chemical compositions of chlorites

The chemical compositions of chlorites are listed in Table 1 (data from Inoue & Utada, 2017). The Mn contents were generally <0.08 a.p.h.f.u. in both the chlorite-G and -B. In an $Al_{(total)}$–(Fe + Mn)–Mg triangle diagram (Fig. 4), the Fe/(Fe + Mn + Mg) ratios varied from 0.08 to 0.55. The ratios in chlorite-B associated with epidote-P were distinctly lower than those in chlorite-G without epidote-P. In the sample at 808.9 m, two compositional populations were observed; relatively Fe-rich chlorite-G stemmed from fillings of early veins and relatively Fe-poor ones where chlorites were partially replaced by illite (Fig. 3c). In the sample at 837.4 m, chlorite-G was rich in Fe, while chlorite-B in a veinlet that crosscut chlorite-G was poor in Fe. Such occurrences indicate that early-formed propylitic chlorite-G altered to chlorite-B during the later-stage potassic alteration. In the sample at 897.7 m, the Fe content in vein-filling chlorite-B depended on the distance from the contiguous epidote-P crystal; the chlorite in the proximal part from the contact of an epidote-P crystal grain was poorer in Fe than its counterpart from the distal part (Table 1 and Fig. 4). The chemical compositions of associated epidotes, K-feldspar, illite, actinolite and titanite can be found in Inoue & Utada (2017). Epidote-P was poorer in Fe than epidote-G. The Mn contents were very low in all the associated minerals.

Estimation of formation temperatures

The $Fe^{3+}/\Sigma Fe$ ratios in Noboribetsu chlorites were not determined separately. Thus, our thermometer, which uses the $Fe^{3+}/\Sigma Fe$ ratios, is not applicable immediately to estimation of the formation temperatures. As mentioned previously, Bourdelle *et al.* (2013) and Lanari *et al.* (2014) proposed semi-empirical thermometers, in which the $Fe^{3+}/\Sigma Fe$ ratios are not required in advance. However, this does not mean that

https://doi.org/10.1180/clm.2018.10 Published online by Cambridge University Press

https://doi.org/10.1180/clm.2018.10 Published online by Cambridge University Press

Table 1. Chemical compositions of chlorites (adapted from Inoue & Utada, 2017).

Depth	792.7 m		808.9 m		837.4 m		880.5 m		837.4 m		897.7 m brownish			
Colour	greenish		greenish		greenish		greenish		brownish		Proximal		Distal	
N	19	STD	21	STD	4	STD	14	STD	16	STD	7	STD	5	STD
SiO_2	28.57	0.61	27.43	0.75	24.97	0.38	27.82	0.51	28.70	0.53	31.17	0.45	29.01	0.31
Al_2O_3	18.01	0.47	17.96	0.82	20.42	0.30	18.19	0.24	18.65	0.42	17.52	0.53	18.97	0.32
TiO_2	0.05	0.06	0.07	0.05	0.05	0.10	0.04	0.05	0.06	0.06	0.05	0.06	0.05	0.06
FeO*	19.45	0.67	26.90	0.96	24.48	0.98	23.41	0.28	15.17	0.36	5.21	0.24	13.32	0.45
MgO	19.08	0.60	13.97	1.19	13.89	0.46	15.74	0.39	20.76	0.45	30.08	0.87	23.55	0.28
MnO	0.59	0.10	0.65	0.11	0.48	0.02	0.67	0.04	0.63	0.07	0.42	0.17	0.58	0.03
CaO	0.13	0.05	0.16	0.06	0.09	0.11	0.23	0.07	0.22	0.06	0.13	0.03	0.08	0.05
K_2O	0.02	0.03	0.07	0.05	0.01	0.02	0.05	0.05	0.04	0.06	0.00	0.01	0.08	0.11
Na_2O	0.10	0.07	0.14	0.12	0.00	0.00	0.04	0.05	0.03	0.04	0.02	0.03	0.01	0.03
Total	85.99	0.94	87.35	1.02	84.38	1.09	86.19	1.10	84.25	1.29	84.59	1.74	85.65	0.83
							O = 14							
Si	2.97	0.03	2.93	0.05	2.74	0.01	2.96	0.02	2.98	0.02	3.05	0.03	2.93	0.01
Al(IV)	1.03	0.03	1.07	0.05	1.26	0.01	1.04	0.02	1.02	0.02	0.95	0.03	1.07	0.01
Σ Tet	4.00		4.00		4.00		4.00		4.00		4.00		4.00	
Al(VI)	1.18	0.03	1.20	0.06	1.37	0.01	1.23	0.02	1.26	0.02	1.07	0.02	1.19	0.03
Mg	2.96	0.07	2.23	0.17	2.27	0.07	2.49	0.04	3.21	0.03	4.39	0.04	3.55	0.03
Mn	0.05	0.01	0.06	0.01	0.04	0.00	0.06	0.00	0.06	0.01	0.03	0.01	0.05	0.00
Fe	1.69	0.07	2.41	0.11	2.24	0.09	2.08	0.03	1.32	0.03	0.43	0.02	1.13	0.03
Ti	0.00	0.01	0.01	0.00	0.00	0.01	0.00	0.00	0.00	0.01	0.00	0.00	0.00	0.00
Σ Oct	5.89	0.02	5.89	0.02	5.93	0.02	5.87	0.01	5.84	0.02	5.92	0.01	5.92	0.02
Ca	0.01	0.01	0.02	0.01	0.01	0.01	0.03	0.01	0.02	0.01	0.01	0.00	0.01	0.01
Na	0.02	0.01	0.03	0.02	0.00	0.00	0.01	0.01	0.01	0.01	0.00	0.00	0.02	0.02
K	0.00	0.00	0.01	0.01	0.00	0.00	0.01	0.01	0.01	0.01	0.00	0.00	0.00	0.00
Fe ratio**	0.36	0.02	0.52	0.03	0.50	0.02	0.46	0.01	0.29	0.01	0.09	0.01	0.24	0.01
Temp (°C)#	235	12	239	11	299	14	220	11	206	11	254	19	253	5
$Fe^{3+}/\Sigma Fe$##	0.199	0.012	0.164	0.024	0.235	0.013	0.186	0.012	0.290	0.024	0.614	0.075	0.304	0.021

*: Total Fe as FeO.
**: Fe/(Fe + Mn + Mg) ratios.
#: Formation temperatures of chlorite estimated by equation 6.
##: estimated $Fe^{3+}/\Sigma Fe$ (see text).

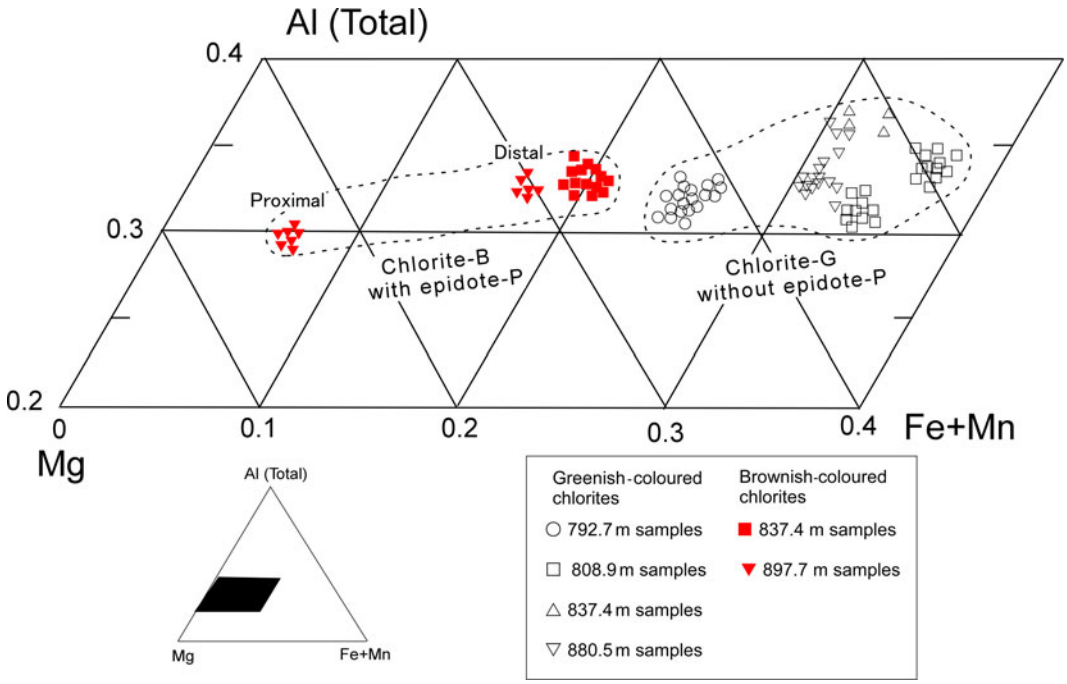

FIG. 4. Plots of chemical compositions of chlorites in part of a triangle diagram of Al (total)-(Fe + Mn)-Mg (modified from Inoue & Utada (2017) and reproduced here with the permission of The Japanese Mineralogical Society).

temperatures estimated by different thermometers are completely consistent with one another. For internal consistency, we calibrated the relation between the temperatures [abbreviated as T (log $K(Fe^{2+}Fe^{3+})$)] estimated by our thermometer and the equilibrium constants (log $K(Fe^{2+})$) were calculated assuming $\Sigma Fe = Fe^{2+}$, using the previous literature data from Niger, Rouez and St Martin (Fig. 5). A fitted curve is:

$$T(^{\circ}C) = 63.83 + 50.41\left[\log K\left(Fe^{2+}\right)\right] + 2.617\left[\log K\left(Fe^{2+}\right)\right]^2 + 2.846\left[\log K\left(Fe^{2+}\right)\right]^3 - 1.097\left[\log K\left(Fe^{2+}\right)\right]^4 + 0.09285\left[\log K\left(Fe^{2+}\right)\right]^5 \left(R^2 = 0.997\right). \quad (6)$$

As a consequence, using equation 6, the average formation temperatures [abbreviated as T (log $K(Fe^{2+})$)] of chlorite-G and -B ranged from 220 to 298°C and from 205 to 258°C, respectively (Table 1). The formation temperatures of chlorite-B at 837.4 m were less than those at 897.7 m but were almost the same for the proximal and distal parts in the sample at 897.7 m. The formation temperatures estimated according to Bourdelle *et al.* (2013) were adopted in our previous work (Inoue & Utada, 2017). Bourdelle's formation temperatures were higher, ~40–80°C more than the values above.

NEDO (1991) documented homogenization temperatures for fluid inclusions in vein quartz or calcite from adjacent propylitic rocks in NB-1. The average values reported were 315°C (range 243–350°C) for quartz in the sample at 767.6 m, 231°C (range 204–257°C) for calcite in the sample at 783.5 m, 235°C (range 208–257°C) for calcite in the sample at 846.6 m and 289 °C (range 266–315°C) for quartz in the sample at 964.6 m. Comparison between the two types of temperature data is impossible, strictly speaking, because of different sampling depths, different minerals used and paragenetic ambiguity. Nevertheless, the reported homogenization temperatures of fluid inclusions appear to be in accordance with the formation temperatures of chlorite estimated by equation 6.

https://doi.org/10.1180/clm.2018.10 Published online by Cambridge University Press

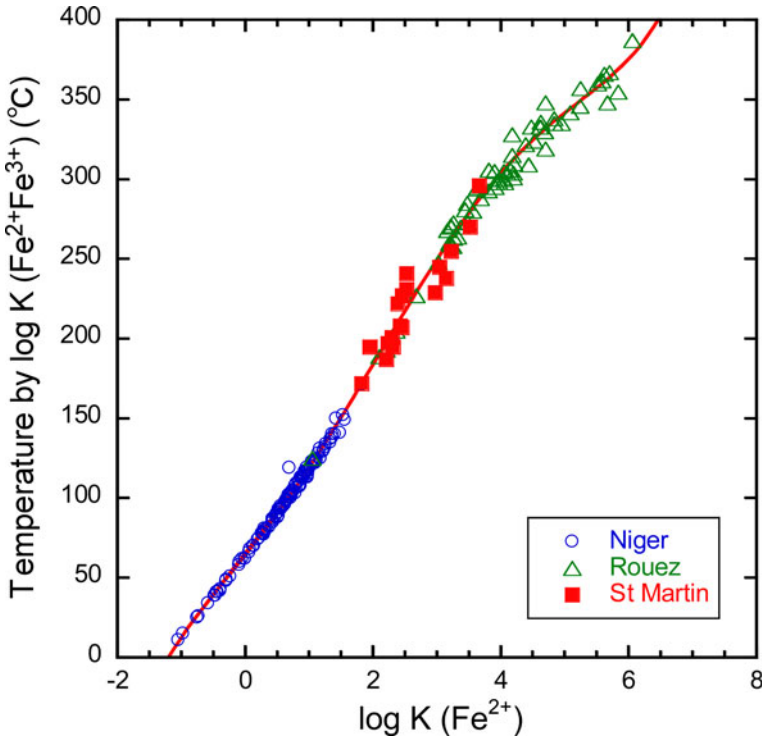

FIG. 5. Relationship between temperature and log $K(Fe^{2+})$ for chlorites from Niger, Rouez and St Martin. The vertical axis represents the temperatures estimated by Inoue *et al.* (2009) taking into account the $Fe^{3+}/\Sigma Fe$ ratios. Log $K(Fe^{2+})$ is the equilibrium constant assuming $\Sigma Fe = Fe^{2+}$.

Pressure conditions for the potassic alteration may be assumed to be under pressures along the vapour-liquid equilibrium curve for water ($P_{sat\ L/V}$) at the above temperatures, possibly at <200 bar.

Estimate of f_{O_2} conditions

It is reasonable to assume that the formation temperatures [T (log $K(Fe^{2+})$)] estimated by log $K(Fe^{2+})$ *via* equation 6 are equal to those [T (log $K(Fe^{2+}Fe^{3+})$)] estimated using the original thermometer proposed by Inoue *et al.* (2009). Then the optimal $Fe^{3+}/\Sigma Fe$ ratios in Noboribetsu chlorites may be obtained by iterative calculations until T (log $K(Fe^{2+})$) = T (log $K(Fe^{2+}Fe^{3+})$). The resulting $Fe^{3+}/\Sigma Fe$ ratios for chlorite-G and -B were, on average, 0.16–0.24 and 0.29–0.48, respectively (Table 1). The ratios exceeded 0.6 in extremely Fe-poor chlorites (the proximal part) in the sample at 897.7 m.

From the estimated $Fe^{3+}/\Sigma Fe$ ratios, in turn, f_{O_2} values were calculated at $P_{sat\ L/V}$ following the method explained in the preceding section (see also the first part of the Appendix). The calculated log f_{O_2} values were plotted as a function of the formation temperature (Fig. 6). Chlorite-G in early-formed propylitic rocks all plotted near the hematite–magnetite equilibrium curve, whereas chlorite-B in the potassic alteration is in the hematite stability field of f_{O_2}. The chlorites in the sample at 897.7 m are separated into two groups according to log f_{O_2}, although the formation temperatures are comparable. Chlorites in the proximal part of the epidote-P crystal formed under more oxidizing conditions than those in the distal part, reflecting the changes in f_{O_2} during crystal growth. Moreover, chlorites formed under more oxidizing conditions have lesser Fe/(Fe + Mn + Mg) and greater $Fe^{3+}/\Sigma Fe$ ratios (Table 1).

Based on the compilation of geothermal fluid compositions, Giggenbach (1987, 1997) indicated that when equilibrium of aqueous fluids and surrounding rocks was attained in geothermal systems, log (f_{H2}/f_{H_2O}) values, defined as R_H, were approximately constant at –2.8 regardless of temperature. The redox

https://doi.org/10.1180/clm.2018.10 Published online by Cambridge University Press

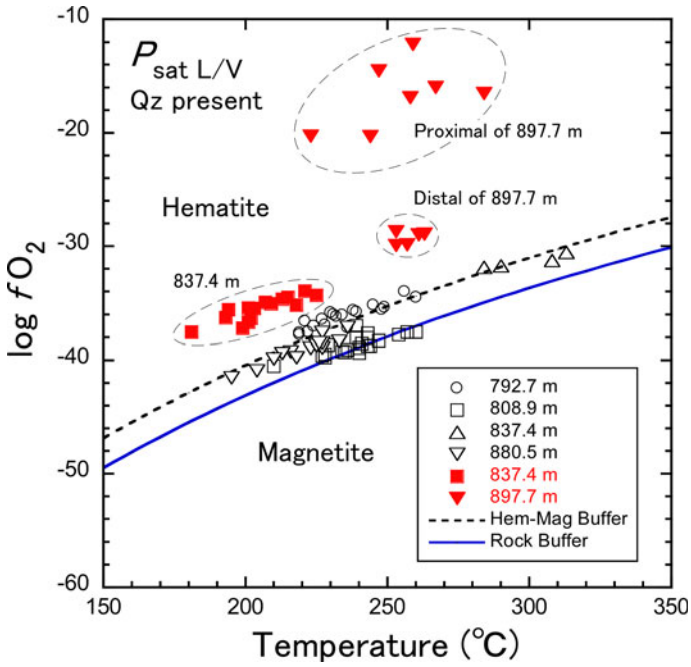

FIG. 6. Plots of estimated log f_{O_2} *vs.* formation temperature for chlorite-B and chlorite-G in Noboribetsu. Dashed and solid curves represent the hematite–magnetite equilibrium calculated at $P = P_{sat\ L/V}$ using thermodynamic data of Lonker *et al.* (1990) and the rock buffer defined by Giggenbach (1997), respectively.

condition R_H was referred to as the 'rock buffer'. Assuming that $R_H = -2.8$, the temperature dependence of log f_{O_2} might be calculated from the relationship: log $f_{O_2} = 5.30 - 25{,}552/T - 2R_H$ (Giggenbach, 1997), where T is temperature in degrees Kelvin. In Fig. 6, chlorite-G is plotted in the area near or slightly above the rock buffer curve, while chlorite-B is in the area far above the rock buffer curve. Assuming that equilibrium of aqueous fluids and minerals was attained in the present system, it follows that the ordinary propylitic assemblage with epidote formed under log f_{O_2} near or slightly lower than the hematite–magnetite equilibrium values, which is rather close to the rock buffer curve. It is conclusive that chlorite-B associated with epidote-P formed under more oxidizing conditions than the ordinary propylitization. Such highly oxidized conditions may be similar to the formation conditions of piemontite in regional metamorphism. Before discussing the log f_{O_2} conditions more quantitatively, however, it is necessary to take into account the effect of water activity. When $a_{H_2O} < 1$, log f_{O_2} decreases as inferred from the equilibrium constant of equation 1, $K_{(1)} = (a_6)(a_{H_2O})^{1/2}/(a_3)(a_{O2})^{1/4}$. The activity of water is unknown in the present system.

Estimate of other chemical conditions

NEDO (1991) documented the composition of fluids recovered from NB-3 (Fig. 2). These fluids may not be the same as those involved in the formation of epidote-P and chlorite-B in NB-1 because the two minerals were not recognized in the potassic alteration zone of NB-3 (Inoue, unpublished data). Nevertheless, taking into account the presence of abundant K-feldspar and illite in the two holes, the chemical conditions in fluid related to the potassic alteration in NB-1 seem to be not largely different from those in fluid recovered from NB-3. The following hypothetical conditions were assumed for the fluid: log $m_{\Sigma S} = -3$, log $a_{K^+} = -3$, ionic strength $(I) = 0.2$ and $a_{H_2O} = 1$ at 250°C, $P_{sat\ L/V}$ and quartz present, where a and m represent activities and molarity of the corresponding chemical species, respectively. As a result the pH of fluid related to the K-alteration was estimated to be ~7 when K-feldspar was in equilibrium with illite (Inoue & Utada, 2017). Note that the pH decreases with increasing ionic strength or a_K^+ (Henley *et al.,* 1984). From the estimated pH, it is in turn inferred that log (a_{K^+}/a_{H^+}) was about 4, and log $(a_{Ca^{2+}}/a^2_{H^+})$ ranged

https://doi.org/10.1180/clm.2018.10 Published online by Cambridge University Press

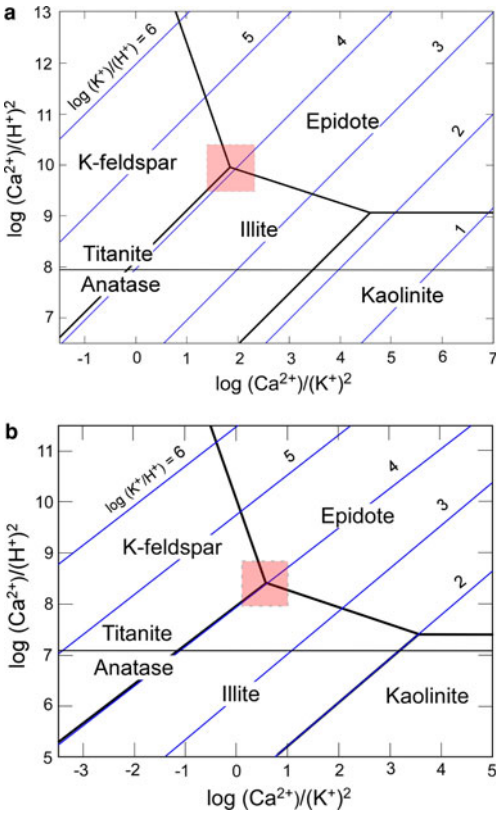

FIG. 7. Log $a(K^+)/a(H^+)$ and log $a(Ca^{2+})/a(H^+)^2$ conditions of K-alteration estimated from mineral assemblages and pH values at (a) 200°C and (b) 250°C, and $P_{sat\ L/V}$; quartz present. Shaded squares are the estimated conditions compatible with the observed mineral assemblages. The thermodynamic data used in the calculations are from Lonker *et al.* (1990).

from 8 to 10 depending on temperature (Fig. 7). These chemical conditions are consistent with the mineral assemblages, epidote-P + K-feldspar + illite + quartz + titanite (+ Mg-chlorite), observed in the samples studied.

Noticeable amounts of sulfide, sulfate and carbonate minerals were not detected inside the veins with epidote-P and chlorite-B. The pyrite in rocks with propylitic alteration was partially replaced by epidote owing to the potassic alteration (Fig. 3d), suggesting that the activity of sulfur, and probably that of CO_2, might be low in hydrothermal fluids related to the potassic alteration. The physicochemical conditions estimated here are, generally, similar to those estimated for many adularia-sericite-type epithermal ore deposits (*e.g.* Heald *et al.,* 1987). However the Fe, S, CO_2 and Cl contents in fluids may be lower than those in epithermal ore-forming fluids. The origin of the oxidized fluid remains unknown.

Effects of fluid composition

It is evident that the Fe/(Fe + Mg) ratio and the Fe^{3+} content in chlorite are related to f_{O_2}, although f_{O_2} is not the only factor to determine the two variables. Beaufort *et al.* (1992) noted that epidotes associated with the Mg-chlorite + hematite assemblage in St Martin were enriched in Fe^{3+} and interpreted that this was due to high f_{O_2} conditions. This is the reverse of the present observation in Noboribetsu whereby the Mg-chlorite+ hematite assemblage coexisting with epidote-P have smaller Fe^{3+} contents than those in epidote-G in adjacent propylitic rocks (Inoue & Utada, 2017). Shikazono (1984) indicated the positive correlation between the Fe^{3+} content in epidote and the Fe_2O_3 content in original rocks. Shikazono & Kawahata (1987) also suggested that there is a positive correlation between the Fe content in chlorite and those in the original rocks and/or fluids. Accordingly the lower Fe contents in both chlorite and epidote in Noboribetsu are due to high f_{O_2} conditions and to the low Fe concentrations in fluids.

Redox buffers in open systems

Veins in hydrothermal alteration are considered as an open system capable of exchanging matter with the external environment. In case that f_{O_2} is controlled externally, there are also two possibilities. If f_{O_2} in fluid is in the magnetite stability field (*i.e.* relatively reduced conditions), the Fe content in chlorite and the modal content of magnetite can be positively correlated with one another, as inferred from the above reaction 5. The relation is compatible with the observations in St Martin (Beaufort *et al.,* 1992). In contrast, if f_{O_2} is in the hematite stability field (*i.e.* relatively oxidized conditions), which is the case in Noboribetsu, the Fe content in chlorite and the modal content of hematite should be inversely correlated, because the structure of trioctahedral chlorite cannot accommodate large amounts of Fe^{3+}. Unfortunately we cannot verify this hypothesis at present because of a lack of information concerning the modal hematite in the Noboribetsu samples.

Limit of Fe^{3+} contents in trioctahedral chlorite

The Fe^{3+} content in chlorite is restricted crystallographically by the structure rather than thermodynamically by ambient f_{O2} conditions (Dyar *et al.,* 1992).

https://doi.org/10.1180/clm.2018.10 Published online by Cambridge University Press

Trivalent cations are more stable in the *M*4 site, which become larger at higher temperatures than the surrounding *M*3 sites, thus limiting the Fe oxidation in chlorite (Nelson & Guggenheim, 1993). Indeed, it has been confirmed by high-angle annular dark field scanning transmission electron microscopic (HAADF-STEM) observation of extremely Fe-rich chlorite that Al with a small ionic radius preferentially occupied the *M*4 site (Inoué & Kogure, 2016). However, the distinction between Fe^{3+} and Fe^{2+} in chlorite was impossible by the HAADF-STEM technique. Also the $Fe^{3+}/\Sigma Fe$ ratios in low-*T* chlorites are generally larger than those in high-grade metamorphic chlorites (*e.g.* Inoue *et al.,* 2009; Lanari *et al.,* 2014; Vidal *et al.,* 2016). This ratio is also related to the total Fe content in chlorite as described previously (Table 1). When the total Fe content in chlorite is <1 a.p.h.f.u., most of the Fe may be ferric in the *M*4 site under highly oxidized conditions. Then, the $Fe^{3+}/\Sigma Fe$ ratio increases significantly as exemplified by chlorites in the Noboribetsu sample at 897.7 m. When total Fe > 1 a.p.h.f.u., however, the excessive Fe must be spread between the *M*1, *M*2 and/or *M*3 sites being mostly ferrous, and consequently the $Fe^{3+}/\Sigma Fe$ ratios may be restricted within a certain limit due to the crystallographic constraints. The limit of Fe^{3+} content that is incorporated in the structure of trioctahedral chlorite is still controversial.

CONCLUDING REMARKS

The present study has demonstrated how to estimate the f_{O_2} conditions and the formation temperatures during chlorite formation by the combination of a semi-empirical chlorite thermometer (Inoue *et al.,* 2009) with the method of Walshe (1986). The present approach, which was applied to the literature data of chlorites from three fields studied previously (Inoue *et al.,* 2009), gave compatible results with those estimated by more rigorous thermodynamic approaches (Vidal *et al.,* 2016). This suggests that the present approach can allow us to discuss qualitatively the changes in redox conditions using the chemical composition of chlorite.

Chlorites, studied for the first time here, occurred as veins and coexisted with pink-coloured epidotes, K-feldspar, illite, quartz and hematite in hydrothermally altered rocks. Applying the present approach to the samples indicated that the chlorites formed under more oxidized conditions than those in adjacent rocks with propylitic alteration. The chemical compositions were characterized by lower Fe/(Fe + Mn + Mg) ratios and larger $Fe^{3+}/\Sigma Fe$ ratios than those in chlorites in adjacent propylitzed rocks. This was attributed to the formation of the mineral assemblage under high f_{O_2} conditions, possibly in association with the low Fe concentrations in the fluid phase. Physicochemical conditions such as *T* and redox estimated using chlorite thermometry, together with the chemical compositions and mineral assemblages, are helpful for achieving a better understanding of the formation process of chlorite during hydrothermal alteration. Nevertheless, the quantitative estimation of $\log f_{O_2}$ requires additional work. In order to understand the role of oxygen during chlorite formation, moreover, we must examine the relationship between the Fe content in chlorite and the modal content of oxide and/or sulfide minerals more accurately. We also need to know, from the crystal chemical point of view, to establish the amount of ferric iron that may enter the chlorite structure.

ACKNOWLEDGEMENTS

The authors are indebted to Alain Meunier, Daniel Beaufort, Patricia Patrier and Philippe Vieillard of Poitiers University, for enthusiastic discussions about chlorite thermometry during a visit by the authors. The initial manuscript was improved by the comments and suggestions of Pierre Lanari and an anonymous reviewer. The authors are also grateful to Takahito Koshiba of Chiba University for his help in making thin sections of rock samples.

REFERENCES

Banno S. & Kanehira K. (1961) Sulfide and oxide minerals in schists of the Sanbagawa and central Abukuma metamorphic terranes. *Japanese Journal of Geology and Geography*, **32**, 331–348.

Beaufort D. (1986) *Definition des equilibres chlorite-mica blanc dans la metamorphisme et la metasomatisme: etude des metasediments encaisant l'amas sulfure de Rouez*. PhD thesis, Université de Poitiers, France.

Beaufort D., Patrier P., Meunier A. & Ottaviani M.M. (1992) Chemical variations in assemblages including epidote and/or chlorite in the fossil hydrothermal system of Saint Martin (Lesser Antilles). *Journal of Volcanology and Geothermal Research*, **51**, 95–114.

Bonazzi P. & Menchetti S. (2004) Manganese in monoclinic members of the epidote group: piemontite and related minerals. Pp. 492–552 in: *Epidote* (A. Liebscher & G. Franz, editors). Reviews in Mineralogy & Geochemistry, **56**, Mineralogical Society of American and the Geochemical Society, Washington, D.C.

https://doi.org/10.1180/clm.2018.10 Published online by Cambridge University Press

Bourdelle F. & Cathelineau M. (2015) Low temperature chlorite geothermometry: a graphical representation based on a T–R^{2+}–Si diagram. *European Journal of Mineralogy*, **27**, 617–626.

Bourdelle F., Parra T., Chopin C. & Beyssac O. (2013) A new chlorite geothermometer for diagenetic to low-grade metamorphic conditions. *Contributions to Mineralogy and Petrology*, **165**, 723–735.

Bryndzia L.T. & Scott S.D. (1987) The composition of chlorite as a function of sulfur and oxygen fugacity: an experimental study. *American Journal of Science*, **287**, 50–76.

Cathelineau M. (1988) Cation site occupancy in chlorites and illites as a function of temperature. *Clay Minerals*, **23**, 471–485.

Cathelineau M. & Nieva D. (1985) A chlorite solid solution geothermometer. The Los Azufres (Mexico) geothermal system. *Contributions to Mineralogy and Petrology*, **91**, 235–244.

Chinner G.A. (1960) Pelitic gneisses with varying ferrous/ferric ratios from Glen Clova, Angus, Scotland. *Journal of Petrology*, **1**, 178–217.

De Caritat P., Hutcheon I. & Walshe J. L. (1993) Chlorite geothermometry: A review. *Clays and Clay Minerals*, **41**, 219–239.

Deer W.A., Howie R.A. & Zussman J. (1986) *Rock-Forming Minerals. 1B. Disilicates and Ring Silicates*. Longman, London, 629 pp.

Dyar M.D., Guidotti C.V., Harper G.D., McKibben M.A. & Saccicia P.J. (1992) Controls on ferric iron in chlorite. *Abstracts of 1992 Annual Meeting of the Geological Society of America*, 338 pp.

Dyar M.D., Guidotti C.V., Holdaway M.J. & Colucci M. (1993) Non-stoichiometric hydrogen contents in common rock-forming hydroxyl silicates. *Geochimica et Cosmochimica Acta*, **57**, 2913–2918.

Essene E.J. (2009) Thermobarometry gone astray. Pp. 101–133 in: *Physics and Chemistry of the Earth's Interior, Crust, Mantle and Core* (A.K. Gupta & S. Dasgupta, editors). Indian National Academy, New Delhi.

Frost B.R. (1991) Introduction to oxygen fugacity and its petrologic importance. Pp. 1–9 in: *Oxide Minerals: Petrologic and Magnetic Significance* (D.H. Lindsley, editor). Reviews in Mineralogy, **25**, Mineralogical Society of America, Washington, D.C.

Giggenbach W.F. (1987) Redox processes governing the chemistry of fumarolic gas discharges from White Island, New Zealand. *Applied Geochemistry*, **2**, 143–161.

Giggenbach W. F. (1997) The origin and evolution of fluids in magmatic-hydrothermal systems. Pp. 737–796 in: *Geochemistry of Hydrothermal Ore Deposits*, 3rd edition (H.L. Barnes, editor). John Wiley & Sons, Inc., New York.

Heald P., Foley N.K. & Hayba D.O. (1987) Comparative anatomy of volcanic-hosted epithermal deposits: acid-sulfate and adularia-sericite types. *Economic Geology*, **82**, 1–26.

Henley R.W. (1984) pH calculations for hydrothermal fluids. Pp. 83–98 in: *Fluid-Mineral Equilibria in Hydrothermal Systems* (R.W. Henley, A.H. Truesdell, P.B. Barton Jr. & J.A. Whitney, editors). Reviews in Economic Geology, **1**, Society of Economic Geology, Texas, USA.

Hillier S. & Velde B. (1991) Octahedral occupancy and the chemical composition of diagenetic (low-temperature) chlorites. *Clay Minerals*, **26**, 149–168.

Inoue A. & Utada M. (2017) Pinkish colored epidotes found in a geothermal exploration well NB-1, Noboribetsu, Hokkaido. *Journal of Mineralogical and Petrological Sciences*, **112**, 147–158.

Inoue A., Meunier A., Patrier-Mas P., Rigault C., Beaufort D. & Vieillard P. (2009) Application of chemical geothermometry to low-temperature trioctahedral chlorites. *Clays and Clay Minerals*, **57**, 371–382.

Inoue A., Kurokawa K. & Hatta T. (2010) Application of chlorite geothermometry to hydrothermal alteration in Toyoha geothermal system, southwestern Hokkaido, Japan. *Resource Geology*, **60**, 52–70.

Inoué S. & Kogure T. (2016) High-angle annular dark field scanning transmission electron microscopic (HAADF-STEM) study of Fe-rich 7 Å–14 Å interstratified minerals from a hydrothermal deposit. *Clay Minerals*, **51**, 603–613.

Jowett E.C. (1991) Fitting iron and magnesium into the hydrothermal chlorite geothermometer. *GAC/MAC/SEG Joint Annual Meeting* (Tront) Abstract, A62.

Kanehira K., Banno S. & Nishida K. (1964) Sulfide and oxide minerals in some metamorphic terranes in Japan. *Japanese Journal of Geology and Geography*, **35**, 175–191.

Kawachi Y., Grapes R.H., Coombs D.S. & Dowse M. (1983) Mineralogy and petrology of piemontite-bearing schist, western Otago, New Zealand. *Journal of Metamorphic Geology*, **1**, 353–372.

Keskinen M. & Liou J.G. (1979) Synthesis and stability relations of Mn-Al piemontite, $Ca_2MnAl_2Si_3O_{12}(OH)$. *American Mineralogist*, **64**, 317–328.

Kranidiotis P. & MacLean W.H. (1987) Systematics of chlorite alteration at the Phelps Dodge massive sulfide deposit, Matagami, Quebec. *Economic Geology*, **82**, 1898–1911.

Lanari P., Wagner T. & Vidal O. (2014) A thermodynamic model for di-trioctahedral chlorite from experimental and natural data in the system MgO-FeO-Al_2O_3- SiO_2-H_2O: applications to P-T sections and geothermometry. *Contributions to Mineralogy and Petrology*, **167**, 968–986.

Lonker S.W., Fitz Gerald J.D., Hedenquist J.W. & Walshe J. L. (1990) Mineral-fluid interactions in the Broadlands-Ohaaki Geothermal system, New Zealand. *American Journal of Science*, **290**, 995–1068.

https://doi.org/10.1180/clm.2018.10 Published online by Cambridge University Press

Miyashiro A. (1965) *Metamorphic Rocks and Metamorphic Belts*. Iwanami-shoten, Tokyo, 458 pp. (in Japanese).
NEDO (1991) The regional report on geothermal development promotion survey, No. 22, *Noboribetsu area*. New Energy Development Organization, 845 pp. (in Japanese).
Nelson D.O. & Guggenheim S. (1993) Inferred limitations to the oxidation of Fe in chlorite: a high-temperature single-crystal X-ray study. *American Mineralogist*, **78**, 1197–1207.
Nesbitt B.E. (1986) Oxide-sulfide-silicate equilibria associated with metamorphosed ore deposits. Part II: Pelitic and felsic volcanic terrains. *Economic Geology*, **81**, 841–856.
Powell R. (1978) *Equilibrium Thermodynamics in Petrology: An Introduction*. Harper & Row, London, 284 pp.
Shikazono N. (1984) Compositional variations in epidotes from geothermal areas. *Geochemical Journal*, **18**, 181–187.
Shikazono N. & Kawahata H. (1987) Compositional differences in chlorite from hydrothermally altered rocks and hydrothermal ore deposits. *The Canadian Mineralogist*, **25**, 465–474.
Thompson J.B., Jr. (1957) The graphical analysis of mineral assemblages in pelitic schists. *American Mineralogist*, **42**, 842–858.
Vidal O., Parra T. & Trotet F. (2001) A thermodynamic model for Fe-Mg aluminous chlorite using data from phase equilibrium experiments and natural pelitic assemblages in the 100 to 600°C, 1 to 25 kbar range. *American Journal of Science*, **301**, 557–592.
Vidal O., Parra T. & Vieillard P. (2005) Thermodynamic properties of the Tschermak solid solution in Fe-chlorite: application to natural examples and possible role of oxidation. *American Mineralogist*, **90**, 347–358.
Vidal O., De Andrade V., Lewin E., Munoz M., Parra T. & Pascarelli S. (2006) P-T-deformation-Fe^{3+}/Fe^{2+} mapping at the thin section scale and comparison with XANES mapping: application to a garnet-bearing metapelite from the Sanbagawa metamorphic belt (Japan). *Journal of Metamorphic Geology*, **24**, 669–683.
Vidal O., Lanari P., Munoz M., Bourdelle F. & De Andrade V. (2016) Deciphering temperature, pressure, and oxygen activity conditions of chlorite formation. *Clay Minerals*, **51**, 615–633.
Walshe J.L. (1986) A six-component chlorite solid solution model and the conditions of chlorite formation in hydrothermal and geothermal systems. *Economic Geology*, **81**, 681–703.
Walshe J.L. & Solomon M. (1981) An investigation into the environment of formation of the volcanic-hosted Mt. Lyell copper deposits using geology, mineralogy, stable isotopes, and a six-component chlorite solid solution model. *Economic Geology*, **76**, 246–284.
Zang W. & Fyfe W.S. (1995) Chloritization of the hydrothermally altered bedrock at the Igarape Bahia gold deposit, Carajas, Brazil. *Mineralium Deposita*, **30**, 30–38.

APPENDIX

The case where the $Fe^{3+}/\Sigma Fe$ ratio is known

In order to explain the calculation procedures, an example of oxide wt.% data determined by EPMA is listed below. The first and second lines in the table correspond to the original data determined by EPMA and the recalculated data assuming $Fe^{3+}/\Sigma Fe$ ratio = 0.26 respectively. FeO* is the total iron, *i.e.* $\Sigma Fe = Fe^{2+}$.

First FeO* is transformed into Fe_2O_3 and FeO using the following relation:

$$Fe_2O_3(\text{wt.\%}) = \frac{\text{FeO}^*(\text{wt.\%})}{\left(\frac{\text{molecular weight of FeO}}{\text{atomic weight of Fe}}\right)} \frac{Fe^{3+}}{\sum Fe} \times \left(\frac{\text{molecular weight of } Fe_2O_3}{2 \times \text{atomic weight of Fe}}\right)$$

$$\text{FeO(wt.\%)} = \text{FeO}^* \times \left(1 - \frac{Fe^{3+}}{\sum \text{Fe}}\right)$$

Then, the structural formula is recalculated based on O = 14. The site fractions of cations and vacancies in the octahedral (oct) and tetrahedral (tet) sites are calculated by, for example, $X_{\text{Mg,oct}} = \text{Mg}/6$, $X_{\text{Si,tet}} = (\text{Si} - 2)/2$, $X_{\text{Al,tet}} = \text{Al(IV)}/2$, following the random mixing model (Inoue *et al.*, 2009). Here Ti, Mn, alkali and alkaline earth elements were ignored in the calculation.

Our thermometer is defined for the following chlorite + quartz assemblage (Inoue *et al.*, 2009):

$$\begin{aligned} &3\text{Sudoite} + \text{Al} - \text{free Chlorite} = \\ &\quad 3\text{Corundophilite(or Amesite)} + 7\text{Quartz} + 4H_2O(l) \\ &3Mg_2Al_3\square Si_3AlO_{10}(OH)_8 + Mg_6Si_4O_{10}(OH)_8 \\ &= 3Mg_4Al_2Si_2Al_2O_{10}(OH)_8 + 7SiO_2 + 4H_2O(l). \end{aligned} \quad \text{(A1)}$$

The equilibrium constant [log $K(Fe^{2+}Fe^{3+})$] of reaction (A1), which takes account of the presence of

https://doi.org/10.1180/clm.2018.10 Published online by Cambridge University Press

Fe^{2+} and Fe^{3+} in structure, is:

$$\log K(Fe^{2+}Fe^{3+}) = 3\log a_{crdp}^{ideal} - 3\log a_{sud}^{ideal} - a_{Afch}^{ideal}, \quad \text{(A2)}$$

where $a_{quartz} = a_{H_2O} = 1$. The ideal terms of activities of endmember components are defined as:

$$a_{Afch} = (X_{Mg,oct})^6 (X_{Si,tet})^2$$

$$a_{crdp} = 45.563 (X_{Mg,oct})^4 (X_{Al,oct})^2 (X_{Al,tet})^2$$

$$a_{sud} = 1728 (X_{Mg,oct})^2 (X_{Al,oct})^3 (X_{vac,oct}) (X_{Si,tet}) (X_{Al,tet})$$

$$a_3 = a_{cham} = 59.720 (X_{Fe^{2+},oct})^5 (X_{Al,oct}) (X_{Si,tet}) (X_{Al,tet})$$

Using the data listed above, $\log K(Fe^{2+}Fe^{3+}) = 1.9509$ is obtained. This value is input in the equation A3, which is a calibration equation proposed by Inoue *et al.* (2009),

$$T(^\circ C) = \frac{1}{0.00293 - 5.13 \times 10^{-4} \log K(Fe^{2+}Fe^{3+}) + 3.904 \times 10^{-5} [\log K(Fe^{2+}Fe^{3+})]^2} - 273.15 \quad \text{(A3)}$$

and the formation temperature, $T(\log K(Fe^{2+}Fe^{3+})) =$ 208°C is obtained.

Walshe (1986) assumed that the ideal activity of H-deficient Fe^{3+}-chlorite component (a_6) approximates the mole fraction of that component (X_6). In practice, it is not easy to calculate X_6. So, when Fe^{3+} was incorporated into the octahedral sites of chlorite, the X_6 was tentatively assumed to be calculated from the relation: $X_6 = Fe^{3+}(1 - F)$, where $F = 28/(28 + Fe^{3+})$. This relation is similar to that of Walshe (1986), and a convenient assumption in the present study. Finally the logarithmic oxygen gas fugacity ($\log f_{O_2}$) can be calculated from

$$\log f_{O_2} = 4\left[(\log a_6 - \log a_3) - \left(-1.926 + \frac{6075.8}{T(^\circ C) + 273.15}\right)\right] \quad \text{(A4)}$$

Here, as $F = 0.966$, we obtain $\log f_{O_2} = -37.7$ from equation A4.

The case where the $Fe^{3+}/\Sigma Fe$ ratio is unknown

The site fractions of cations and vacancies in each site, except for Fe^{3+}, are calculated by the same manner as above, using the data below.

Then the logarithmic equilibrium constant [$\log K(Fe^{2+})$] of reaction A1 is calculated:

$$\log K(Fe^{2+}) = 3\log a_{crdp}^{ideal} - 3\log a_{sud}^{ideal} - a_{Afch}^{ideal}$$

Put the equilibrium constant (= 2.4198) into the equation 6 in the text and the formation temperature, assuming $\Sigma Fe = Fe^{2+}$: $T(\log K(Fe^{2+})) = 211.5$°C, is obtained. The difference in estimated temperature for the St Martin sample was derived from the statistical error between the two calibration curves. Furthermore, by iterative calculations until $T(\log K(Fe^{2+})) = T(\log K(Fe^{2+}Fe^{3+}))$, we can obtain the optimum $Fe^{3+}/\Sigma Fe$ ratio. In turn, we calculate a_3 and X_6 following the same path as above, and finally estimate $\log f_{O_2}$ based on equation A4. The predicted $Fe^{3+}/\Sigma Fe$ ratio increased with decreasing Fe/(Fe + Mn + Mg) ratio in chlorite, but the resultant $\log f_{O_2}$ did not change significantly with the $Fe^{3+}/\Sigma Fe$ ratios.

https://doi.org/10.1180/clm.2018.10 Published online by Cambridge University Press

https://doi.org/10.1180/clm.2018.10 Published online by Cambridge University Press

Sample	$Fe^{3+}/\Sigma Fe$	SiO_2	Al_2O_3	TiO_2	FeO*	FeO	Fe_2O_3	MgO	MnO	CaO	Na_2O	K_2O	Total
St Martin		27.57	20.03	0.13	22.17			15.81	0.79	0.18	0.02	0.05	86.75
	0.26	27.57	20.03	0.13		15.52	7.39	15.81	0.79	0.18	0.02	0.05	87.49
					O = 14								
Structural formula	Si	Al(IV)	Ti	Al(VI)	Fe^{2+}	Fe^{3+}	Mg	Mn	Σoct	Vacancy			
	2.83	1.17	0.01	1.25	1.33	0.57	2.42	0.07	5.57	0.43			
Site fraction Activities	$X_{Mg,oct}$	$X_{Al,oct}$	$X_{Fe2+,oct}$	$X_{Fe3+,oct}$	$X_{vac,oct}$	$X_{Si,tet}$	$X_{Al,tet}$	a_{Afch}	a_{crdp}	a_{sud}	log K	T(°C)	
	0.403	0.208	0.222	0.095	0.072	0.415	0.585	0.0007	0.0178	0.0446	($Fe^{2+}Fe^{3+}$) 1.9509	208	

Sample	SiO_2	Al_2O_3	TiO_2	FeO*	FeO	Fe_2O_3	MgO	MnO	CaO	Na_2O	K_2O	Total	
St Martin	27.57	20.03	0.13	22.17			15.81	0.79	0.18	0.02	0.05	86.75	
					O = 14								
Structural formula	Si	Al(IV)	Ti	Al(VI)	Fe^{2+}	Fe^{3+}	Mg	Mn	Σoct	Vacancy			
	2.89	1.11	0.01	1.36	1.94		2.47	0.07	5.77	0.23			
Site fractions Activities	$X_{Mg,oct}$	$X_{Al,oct}$	$X_{Fe2+,oct}$	$X_{Fe3+,oct}$	$X_{vac,oct}$	$X_{Si,tet}$	$X_{Al,tet}$	a_{Afch}	a_{crdp}	a_{sud}	log K	T(°C)	$Fe^{3+}/\Sigma Fe$
	0.423	0.226	0.323		0.039	0.442	0.557	0.0011	0.0231	0.0347	(Fe^{2+}) 2.4198	211.5	0.26